이학석사 학위논문

Blocking effect in CsI(Tl) crystal by neutron

CsI(Tl) 결정 내부에서의 중성자에 의한 블로킹 효과

2013 년 8 월

서울대학교 대학원

물리천문학부

주 한 울

Blocking effect in CsI(Tl) crystal by neutron

CsI(Tl) 결정 내부에서의 중성자에 의한 블로킹 효과

지도 교수 최 선 호

이 논문을 이학석사 학위논문으로 제출함
2013 년 8 월

서울대학교 대학원
물리천문학부
주 한 울

주한울의 이학학사 학위논문을 인준함
2013 년 8 월

위 원 장 _____ (인)

부위원장 _____ (인)

위 원 _____ (인)

학위논문 원문제공 서비스에 대한 동의서

본인의 학위논문에 대하여 서울대학교가 아래와 같이 학위논문 제공하는 것에 동의합니다.

1. 동의사항

① 본인의 논문을 보존이나 인터넷 등을 통한 온라인 서비스 목적으로 복제할 경우 저작물의 내용을 변경하지 않는 범위 내에서의 복제를 허용합니다.

② 본인의 논문을 디지털화하여 인터넷 등 정보통신망을 통한 논문의 일부 또는 전부의 복제.배포 및 전송 시 무료로 제공하는 것에 동의합니다.

2. 개인(저작자)의 의무

본 논문의 저작권을 타인에게 양도하거나 또는 출판을 허락하는 등 동의 내용을 변경하고자 할 때는 소속대학(원)에 공개의 유보 또는 해지를 즉시 통보하겠습니다.

3. 서울대학교의 의무

① 서울대학교는 본 논문을 외부에 제공할 경우 저작권 보호장치(DRM)를 사용하여야 합니다.

② 서울대학교는 본 논문에 대한 공개의 유보나 해지 신청 시 즉시 처리해야 합니다.

논문제목 : Blocking effect in CsI(Tl) crystal by neutron

학위구분 : **석사 □ · 박사 □**
학 과 : 물리천문학부
학 번 : 2011-23281
연 락 처 : hwjoo1240@gmail.com
저 작 자 : 주 한 울 (인)

제 출 일 : 2013 년 8 월 2 일

서울대학교총장 귀하

Blocking effect in CsI(Tl) crystal by neutron

supervisor

Seon Ho Choi

Thesis by

Ju, Han-wool

In Partial Fulfillment of the Requirements

For the Degree of

Master of Science

August 2013

Department of Physics & Astronomy

Seoul National University

Abstract

To detect WIMP directly, which is strong candidate for dark matter, KIMS collaboration used CsI(Tl) crystal as a scintillation detector. To increase the detector`s sensitivity, we studied channeling and blocking effect in the CsI(Tl) crystal, which refer to the orientation dependence of charged ion`s penetration in crystals. It results in modulation of scintillation or ionization yield in the CsI(Tl) crystal.

In order to measure the channeling and blocking effect in CsI(Tl) crystal, we used a CsI(Tl) crystal, a neutron generator, and three neutron detectors, with making the directions of recoil ions induced by the neutron-nucleus scatterings to be aligned along one of the symmetry axis or plane in the CsI(Tl) crystal. Also, we did simulations to compare their results with the data obtained from our experimental setup, by two kinds of computer simulations, MARLOWE and Geant4. To confirm the affection of the blocking effect in the CsI(Tl) crystal, we compared the light yields of recoil ions moving along the symmetry axis, [110], and those of recoil ions moving along random directions, and compared mean decay time of signals from each recoil direction. By comparing those from experiments and simulations, we could find a clue for the blocking effect which is expected to result in less scintillation light yields.

Keywords : Dark matter, WIMPs, KIMS, CsI(Tl) crystal, Channeling effect, Blocking effect, Scintillation

Student Number : 2011-23281

Contents

List of Figures

List of Tables

Chapter 1

Introduction

1.1. CsI(Tl) crystal as a dark matter detector

Dark matter is a kind of matter which is distributed all over the universe and it accounts for a large part of total mass of the universe. According to the Planck mission team, and based on the standard model of cosmology, the total mass-energy of the universe contains 4.9% of ordinary matter, 26.8% of dark matter, and 68.3% of dark energy. [1] Thus, dark matter is estimated to constitute 84.5% of the total matter of the universe and 26.8% of the total content of the universe. Because dark matter does not interact with ordinary matter by electromagnetic forces, it does not emit or absorbs light or other electromagnetic radiation, so we cannot see dark matter directly. Instead, we can infer its existence and properties from its gravitational effects on visible matter, radiation, and large-scale structure of the universe.

The existence of dark matter was first postulated by Fritz Zwicky, in 1933. [2] In 1932, Jan Oort found that the orbital velocities in the Milky Way do not decrease with increasing distance from the galactic center, and in 1933, Fritz Zwicky suggested the existence of dark matter, based on the measured motions of galaxies in the Coma cluster. Subsequently, many other observations have indicated the presence of dark matter in the universe, including the rotational speeds of galaxies by Vera Rubin, in the 1960s-1970s, gravitational lensing of background objects by galaxy clusters such as the Bullet Cluster, the temperature distribution of hot gas in galaxies and

clusters of galaxies, and more recently the pattern of anisotropies in the cosmic microwave background.

According to the theory of super symmetry, one of the most probable candidates for dark matter is Weakly Interacting Massive Particle (WIMP). [3] [4] It has similar properties with the model of a relic dark matter particle from the early universe, when all particles were in a state of thermal equilibrium. It interacts with ordinary materials only through gravity and the weak force, and it has weak scale of interaction cross sections and large masses in the GeV-TeV range.

Direct detection of WIMP particle is based on detection of nuclear recoil energies in a target detector material. When WIMPs interact with ordinary nuclei in the target detector material, the material emits absorbed energy by ionization, scintillation or phonon. We can obtain information about WIMP-nucleon elastic scattering from material`s responses like these. Here, because the nuclear recoil energies are typically less than 100 keV, the target detector material is recommended to be an active detector that can measure such a small energy deposition. Therefore, for the target detector material, elements which have large cross section for WIMP interaction are preferred. Because WIMPs interact with ordinary matter very weakly, WIMP-nucleon scattering events rarely occur, so we need high sensitive detector to detect the nuclear recoils with low radioactive background level for direct detection of WIMPs. Sensitivity of WIMPs detection depends on various parameters of the detector, such as, detection threshold, mass of the detector, background rate, pulse shape discrimination (PSD) capabilities, etc. As a detector material that satisfies above conditions, crystal scintillators, such as NaI or CsI are in use because sodium, cesium and iodide ions are good target for WIMP interaction due to its good sensitivity to the spin dependent/independent interactions of WIMPs. Moreover, because pure NaI or CsI crystals without doping are not very efficient scintillators at room temperature, a small amount of impurity atoms, such as thallium or sodium are added as luminescent centers.

NaI(Tl) crystal is more popular detector material than CsI(Tl) crystal, because of contamination by radioactive isotopes of Cs and its lower light yields than NaI(Tl) crystal. But KIMS (Korea Invisible Mass Search) solved

these problems by developing radio-pure CsI(Tl) crystal and adapting PMTs with green-enhanced photocathodes, instead of normal bi-alkali photo-cathodes, to improve the number of photoelectrons. Since CsI(Tl) crystal has good scintillation properties and large light yields, it is suitable for low-energy measurement and it has low background rate because of its relatively good PSD capability. Moreover, it is easy to fabricate detectors with large volume, because the crystals are not hygroscopic (Tl-doped case) or less hygroscopic (Na-doped case) compared to NaI crystal, and the large masses of Cs and I nuclei enhance the cross-section for WIMP-nucleus scattering, spin independent interaction. From the above properties of CsI(Tl) crystal, we can conclude that CsI(Tl) crystal is sufficiently good detector material for direct dark matter detection.

1.2. Channeling and Blocking Effect on the CsI(Tl) crystal

The channeling and blocking effect in the crystals refer to the orientation dependence of charged ion`s penetration in the crystals.

The channeling effect is characterized as maximum penetration range, maximum scintillation or ionization yield, and minimum scattering yield when an incident ion moves through the empty space between symmetry axes or planes in a mono crystalline target. This effect occurs when the nucleus, which recoils after being hit by a WIMP particle, moves off in a direction close to a symmetry axis or symmetry plane of the crystal. The channeled ions suffer a series of small-angle scatterings with nuclei at lattice sites, and that makes the channeled ions remain in the opened “channels” between the rows or planes of lattice atoms. Thus they penetrate much further into the crystal than in other directions, and transfer almost of their energy to electrons, transferring more energy than to nuclei, producing phonons and producing more scintillation and ionization. In scintillators like NaI(Tl) or CsI(Tl), channeling effect increases the observed scintillation light output correspond to particular recoil energy.

In contrast, the blocking effect is large-angle interactions of projectile particle with the nuclei at lattice sites, directly in front of the recoiling nucleus site. The blocking effect occurs for charged particles whose

trajectories start from lattice sites inside a crystal. They undergo large angle scatterings when their direction is along the symmetry axis or plane. Here, from a practical standpoint, 'the charged particles' imply either the emission of particles from nuclei in the crystal atoms or the large-angle Rutherford scattering of incident beam particles. Since the impact parameters involved in large angle scattering are several orders of magnitude smaller than the zero-point thermal-vibration amplitudes for atoms in crystals, there usually is no practical difference between the two types of particle emission. A typical experimental arrangement for a blocking measurement is shown in Fig.1.1. Beam of the particles is incident upon a mono-crystal in a random direction and a tightly collimated detector measures particles emerging at an angle Ψ with respect to a high-symmetry crystal direction. The blocking measurement consists of determining the yield of emitted particles as a function of Ψ, as Ψ is varied (usually by moving the detector) over a small range centered about $\Psi = 0$. When the collimated detector is located on a major crystal direction ($\Psi = 0$), the detected yield of emerging particles is a minimum; as Ψ is increased, the detected yield rises.

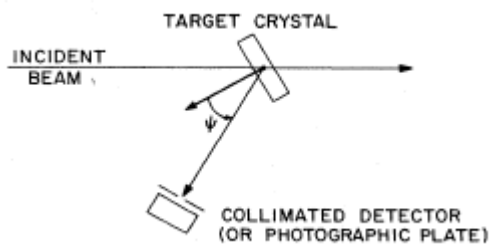

Figure 1.1 : Schematic arrangement for a typical blocking measurement.

Here, the function of the incident beam is merely to create particles that emerge from lattice sites, so the incident beam does not need to be tightly collimated, nor need it consist of charged particles. Collimation becomes important when one wishes to define the recoil direction of compound nuclei formed in nuclear reactions induced by the incident beam. Detailed experimental setup will be mentioned in next chapter.

These effects have received a large amount of attention to interpret

experiments searching for WIMPs through their scattering in a low-background detector and are applied for many other areas such as, crystallography, ion implantation, production of the polarized beam, measurements of the lattice disorder or of short nuclear life times, and so on. (see for example [5, 6, 7])

1.3. Daily and Annual modulation for WIMP research

The channeling and blocking effects is important for confirming daily and annual modulation for WIMP research. Because these two effects are direction-dependent effects, and the "WIMP wind" is expected to arrive to Earth on average from a particular direction fixed to the Galaxy, the Earth`s revolution and rotation can change the direction of the "WIMP wind" with respect to the detector crystal`s axes, thus daily and annual modulation of the dark matter signal can be observed via changes in scintillation or ionization.

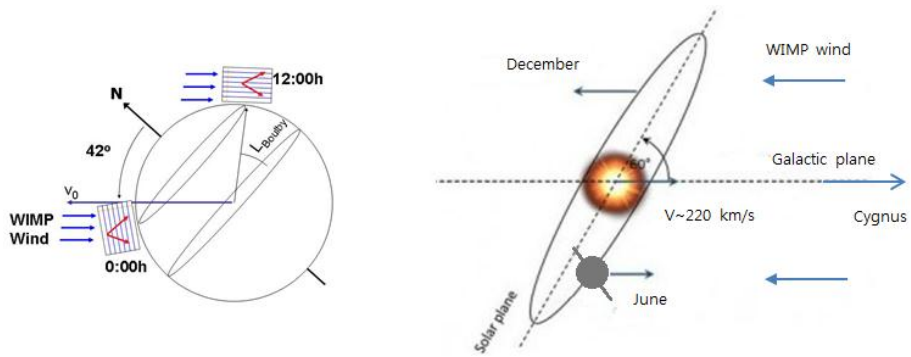

Figure 1.2 : Daily (left) and annual (right) modulation of a WIMP signals caused by Earth`s revolution and rotation [8][9]

1.4. Motivation

Our study about the channeling and blocking effect starts from the claim by DAMA, another research group of researching dark matter, that KIMS detector loses some nuclear recoil events because of the channeling effect and their pulse shape discrimination (PSD) cut, which is event selection cut

to remove the gamma backgrounds. [10] They claimed that recoil ions moving along to the symmetry axis would experience the channeling effect and their scintillation yield would be increased as gamma backgrounds. As a result, the event is removed by PSD cut. But in their study, they overestimated the channeling fraction because they did not consider the blocking effect. [11] [12] Since there is no experiment to see the channeling and blocking effect in the scintillation detector for heavy recoil ions like Cs and I, we decided to use a numerical simulation program to compare with the experimental data.

In chapter 2, we will introduce the experimental setup to measure the channeling and blocking effect and the data acquisition method and the analysis method. In chapter 3, we will introduce the simulation programs we used. In chapter 4, we compared the result of this experiment with the result of previous Dr. Ju-hee Lee`s experiment about channeling effect [12], and with MC data obtained from MARLOWE and Geant4 simulation.

Chapter 2

Experiment

2.1. Goal of this experiment

In order to measure the channeling and blocking effect in our crystal, we make the directions of recoil ions induced by the neutron-nucleus scatterings to be aligned along one of the symmetry axis or plane in the CsI(Tl) crystal. The setup is similar with the Dr. Ju-hee Lee`s experiment for the channeling effect in the CsI(Tl) crystal [12], but there was miscalculation in the CsI(Tl) crystal`s position, so the crystal`s height was 1 cm lower than we expected, and the table we set the CsI(Tl) crystal and neutron detectors was not flat, but it was not considered in previous experiment. So, there was ±1° of uncertainties for the alignment of neutron detectors, which are correspondent to the 0.4 keV recoil energy deviation.

In this experiment, due to the channeling or blocking effect, we expect that we measure the different measured energy, E_{meas} spectra in the CsI(Tl) crystal when we select events tagged by different neutron detectors, which have the same scattering angles but different azimuthal angles on the bottom plane of a cone in Fig. 2.4. By comparing the results with the reproduced E_{meas} from MARLOWE and Geant4 with considering the equivalent setup, we test our scintillation model and the estimation for the channeling and blocking effect.

2.2. Experimental Setup

2.2.1. Neutron Generator

In this experiment, we used neutrons as projectile particles. Neutrons are generated from a portable neutron generator MP320 made by Thermo Fisher Scientific Company, which emits 2.4 MeV mono energy neutrons by deuterium-deuterium collisions. The neutron generator is composed of an accelerator tube and an electronics part. They are connected with BNC cables. The electronics part plays a role to supply low voltages for the ionization and high voltages, 90 keV at maximum, for the acceleration of deuterium. The accelerator tube is filled with sulfur hexafluoride gases with over 8 atmospheric pressures and is electronically dry, and there are two Zirconium materials as deuterium reservoirs at both sides, which play roles as an ionized deuterium supplier and as a deuterium target plane, respectively. When we induce negative high voltage between each ends of the accelerating tube by electronics part, the ionized deuterium is attracted to the deuterium target plane and their collision will produces neutrons almost isotropically as the following process, but the processes below are detained in the target plane due to the negative voltage. The flux is around 10^6 per a second.

$$
\begin{aligned}
{}^{2}_{1}H + {}^{2}_{1}H \rightarrow\ & {}^{1}_{0}n + {}^{3}_{2}He + 3.27\ MeV \quad (50\%) \\
\rightarrow\ & {}^{1}_{1}p + {}^{3}_{1}H + 4.03\ MeV \quad (50\%)
\end{aligned}
$$

We shielded the neutron generator with 10 cm thickness-polyethylene box and a 10 cm thick-lead wall like Fig.2.1, except for a 3.2 cm diameter window to extract neutrons, to block high energy gammas from the deuterium fusion inside the accelerator tube. Furthermore, because there were unexpected events, which will be mentioned in chapter 4, and we suspected that these events as X-ray from the neutron source, Zirconium, so we tried to remove these events by blocking neutron beam line with a 2.5cm lead block. After blocking neutron beam line with a lead block like ① in Fig.2.1 and Fig.2.2, it seems that the problem is solved, but after few weeks,

these events appeared again. So we put some more lead blocks like ② in Fig.2.1 and Fig.2.2. After that, almost of the unknown events near 30 keV are disappeared. The result will be shown in Fig. 4.1 (b).

The operation for the neutron generator is done by a distant computer from the shielding box for the safety, which is connected to the generator by serial port, and controls the generator by a Graphic User Interface (GUI) program. We modulate five parameters on the menu, the beam current, the high voltage, pulse frequency and its duty time, and the total run time. The maximum neutron flux comes out at the combination of 60 μA and 90 kV for the beam current and the high voltage respectively. However, since the gamma flux also increase, we measured the flux ratio between neutrons and gammas, $\frac{f_{neutron}}{f_{gamma}}$, with changing the combination. When we set the larger beam current, we get the higher neutron flux. So we fix the beam current to 60 μA, and with changing the high voltage, we get the highest flux ratio at 50 kV, which is about 2.

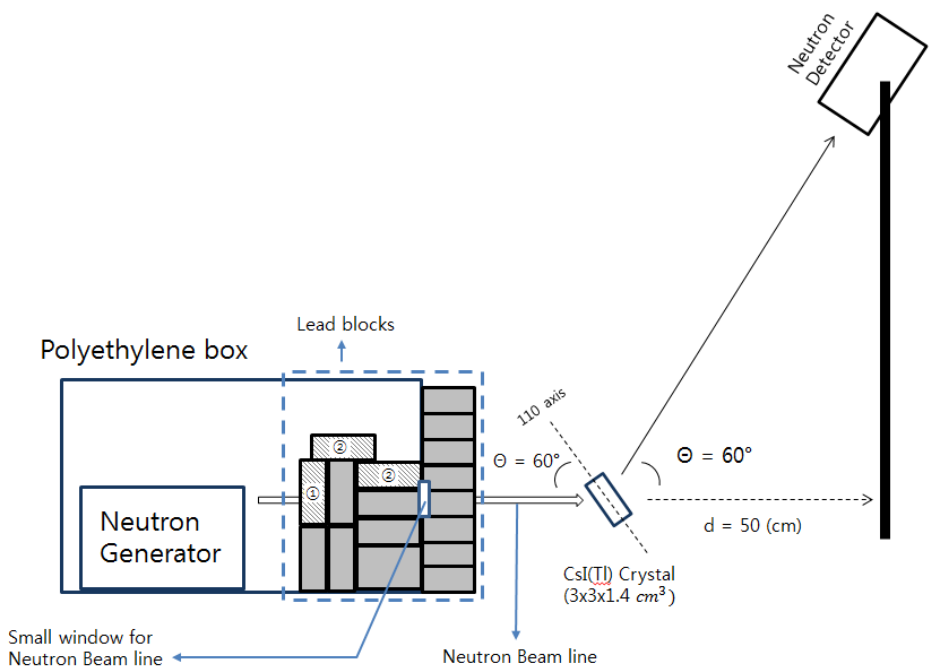

Figure 2.1 : Simple description of experimental setup (Side view)

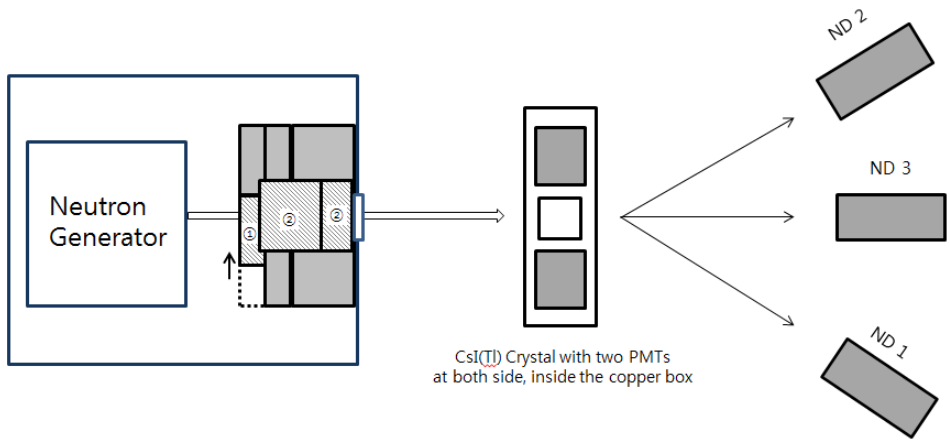

Figure 2.2 : Simple description of experimental setup (Upper view)

2.2.2. CsI(Tl) crystal

As shown in Fig.2.2, the target material, CsI(Tl) crystal is located at the center position and is covered by a copper box which has the thickness of 1mm, and there are 2 PMTs at both sides of the crystal. We used PMT 9269QA for the CsI(Tl) crystal, a green extended PMT, to improve the number of photoelectrons, and PMT R329-02 for neutron detectors. The CsI(Tl) crystal has dimensions of 3 x 3 x 1.4 cm^3 and its doping levels are under 0.1 mole % for Thallium, and it is wrapped by a VM2000 reflector of 64 micrometer and a Teflon tape of 0.5 mm. We measured the three planes of the crystal by X-ray diffraction (XRD) measurement which is requested to Center for Materials Analysis in Seoul National University. In XRD measurement for the CsI(Tl) crystal we are using, the 2θ distribution result shows three peaks only in one plane, of which angles are 27.6°, 57°, and 91.4°. These represent (110), (220) and (411) for each plane and it shows that the crystal had grown to be mono-crystalline well. However, the other planes show no peak. This implies that the crystal was cut along the plane of non-symmetry, but the probability that the crystal is mono-crystalline is larger than those with many peaks. Crystals are usually grown along a [110]

or a [111] axis. So (110) plane of this crystal might be obtained by the cut in parallel with crystal growing direction. Thereby we measured the blocking effect with aligning the [110] direction which is the normal vector of the (110) plane to the one of the recoil directions.

In order to convert the light yield from the scintillation detector to E_{meas}, which is the electron equivalent energy, the energy calibration is needed. We did energy calibration with 59.54 keV gammas from ^{241}Am source to reproduce measured energy for every 3 days with rerunning the neutron generator. In this CsI(Tl) calibration, we used event selection cuts. Two cuts are same with those applied to the nuclear recoil event in the channeling and blocking effect experiment, which are (1) and (2) of Table 2.2 and will be explained in section 2.3 in detail. Fig.2.3. shows the result of the calibration.

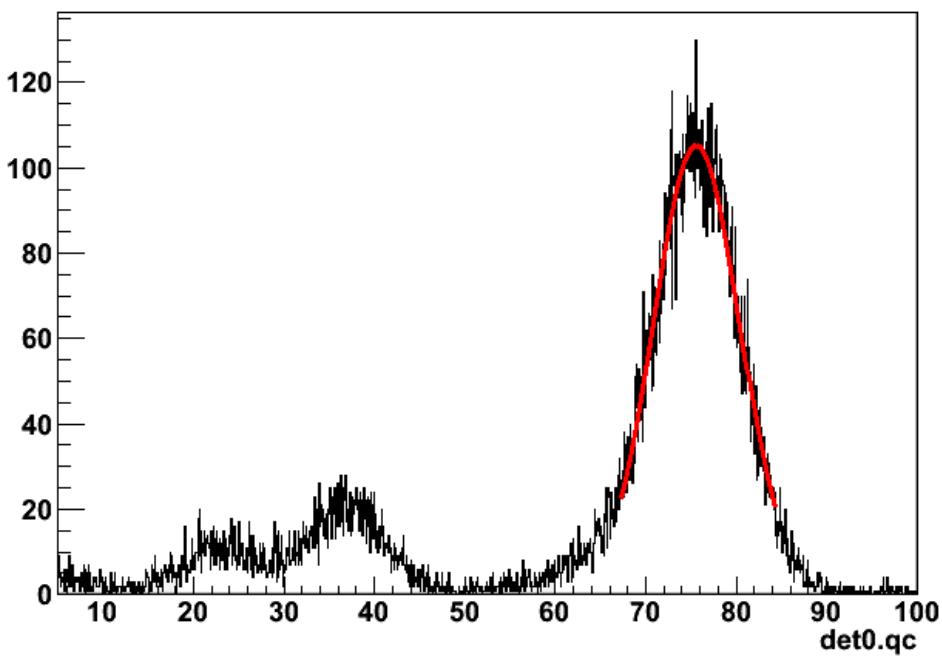

Figure 2.3 : Result of the energy calibrations with ^{241}Am source. Horizontal axis is total ADC sum from two PMTs at both sides of the CsI(Tl) crystal.

2.2.3. Neutron Detector

In order to detect neutrons after scattering with the nucleus in CsI(Tl) crystal, we set three neutron detectors like Fig.2.4. These are made of BC501a, the name of the liquid scintillator, which has the highest discrimination power for the neutron and gammas. However, it has the flash point at 24 ℃, and it is toxic and volatile. Besides, it is easily oxygenated and denatured, when the sealing of its bottle is not enough. So the protection of its leakage is most important thing in terms of the safety and the discrimination power. The attached PMTs and the high voltages for the neutron detectors are listed in Table 2.1.

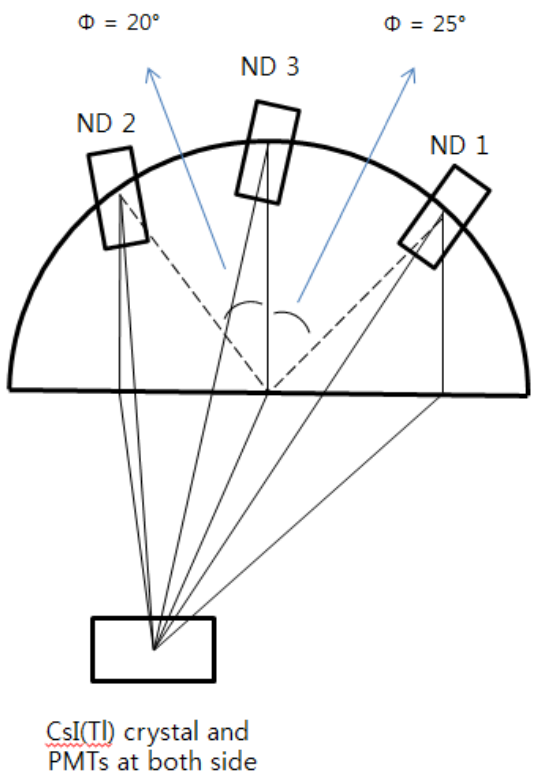

Figure 2.4 : Setup of neutron detectors with the same scattering angles of 60 °, and with different azimuthal angles of Φ = 0°, -20° and 25 °.

Name	Part number	ALS [a] (A/lm)	ADC [b] (nA)	HV [c] (V)	Peak [d]
ND1	RD5404	427	0.42	2103.4	0.380
ND2	RD5101	248	0.52	1661. 6	0.328
ND3	RD5101	892	1.5	1436.4	0.432

Table 2.1 : Photomultiplier tubes used for the neutron detectors [e]

[a] Anode Luminescence Sensitivity
[b] Anode Dark Current
[c] The used high voltage of each PMT
[d] The peak position near the Compton edge in ADC sum distribution
[e] All are the model of H6410 and R329-02 manufactured by HAMAMATSU [13].

For the discrimination of recoil directions, we should put the neutron detectors far from the CsI(Tl) crystal to reduce their solid angles. They have the same scattering angles of 60 ° and the different azimuthal angles Φ of =0°, -20° and 25° respectively. To align recoil directions on a symmetry axis, [110], we tilted CsI(Tl) crystal like Fig. 2.5. So the central positioned neutron detector, ND3 in Fig.2.4, would see the neutrons of which recoil ions go straight to the next target and undergo a large angle scattering, thereby the light yield may also be decreased in CsI(Tl) crystal. The solid angle is ~ 0.2 msr and the recoil angle deviation for the single elastic scattering is ± 3° in the GEANT4 simulation. From the MARLOWE simulation, up to ± 5° deviations the recoil directions are subject to the blocking effect. For multiple scattering and inelastic scattering, the angle deviations of recoil ions are larger than that of single scattering, but since the fraction of the total events is several %, ND3 is expected to usually see neutrons related to the blocking effect. So we compare each E_{meas} distribution for the three neutron detectors in 60° setup. Each detector is composed of Bc501a liquid scintillator, which has highest PSD power for

the neutrons and gammas, and a double-layered-bottle of Teflon and stainless steel, whose thickness is 5mm respectively, are surrounding the crystal and the detectors are supported by aluminum profiles and a camera mount, which is available to modulate the angle and stands 50 kg at maximum. We set the profiles and neutron detectors by using laser pointer. First, we set the distance between bottom of the neutron detector 3 and CsI(Tl) crystal as 0.5m, and calculated the height of center of the detectors at Φ=0°, -20°, 25° on the same bottom plane of a cone, and calculated angles between floor and detectors. After that, we set the laser pointer with the angle and direction as we calculated, and set the profiles and the neutron detectors with fitting small hole of the neutron detector and laser from the laser pointer.

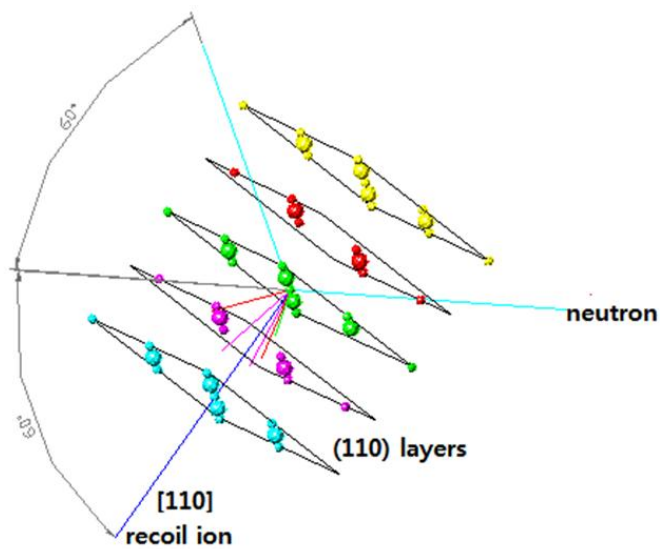

Figure 2.5 : The scheme of (110) layers of CsI(Tl) crystal and one of the trajectory of a neutron and a recoil ion in the layers tilted by 60° to the central direction of the incident neutrons

	Name	Example
(1)	Fit Quality(FQ) cut	FQ < 2.5
(2)	Second time(t1) cut	det0.t1 > 2.5
(3)	Start time difference cut	pmt30.t0 – det0.t0 < 0.1 (det0.Eqc≤5) -0.1 < pmt30.t0 – det0.t0 < 0.1 (det0.Eqc>5)
(4)	Single hit cut	Only 1 detector has the signal

Table 2.2 : Event selections cuts. When all cuts are satisfied, an event is accepted as a candidate of nuclear recoils. After these cut, PSD cut is applied to discriminate events as Surface Alpha, neutron and gamma induced ones.

2.3. DAQ and event selection

To obtain data, we used two kinds of modules, linear Fan In/Out in NIM module and two Flash Analog to Digital Converters (FADCs) in VME module, like Fig.2.6. The electronic signals and their time information from the neutron detectors and the PMTs at both side of the CsI(Tl) crystal go to each FADC in a VME crate, and when the signals from PMTs and neutron detectors satisfy some conditions, then the combined channels in FADC generate triggers. For signals from PMTs, trigger is generated when there are more than two pulses in each PMT or a large peak of over 300ns width in a PMT. For signals from neutron detectors, trigger is generated when there is a single pulse larger than 40 mV and over 10 ns of the pulse width, of which equivalent ADC sum is much lower than 0.15 that is our event cut value. One of the triggers from the FADC used for neutron detectors goes to the Fan IN/OUT module and converted from a TTL signals to analog signals in the inverse mode. The inversed signals go to the another channel of CsI(Tl) in FADC module, and when these signals are gathered in a 2 μs window, there comes the final trigger out. It is distributed to the two FADCs through trigger in, and the signals are filter by these triggers, and the filtered events are transported to the PC and stored.

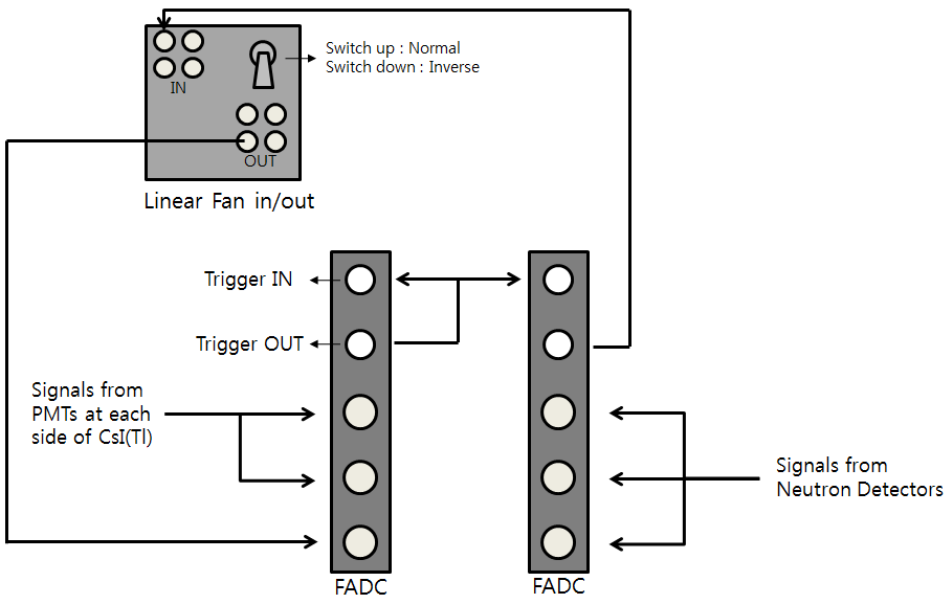

Figure 2.6 : The trigger system for DAQ.

After DAQ, we did event selections to remove background signals from PMTs and to pick out neutron events. Events cuts we used in our experiment are listed in table 2.2. Fit quality cut is the cut to remove events from one of the dominant background signal, randomly dispersed pulse. These signals appears due to the high energy gammas from inelastic scatterings or neutron capturing by ion in CsI(Tl) crystal. When we fit pulses in an event with an exponentially decay function, we can remove most of them. Time coincident cut selects events whose start time difference between signals from CsI(Tl) crystal and signals from one of the three neutron detectors are within 100 ns. But for the events of lower than 5 keV energy, the cut is not applied because the start time of CsI(Tl) pulses have larger deviations in the low energy region. After the event selections, we applied the last event selection cut, the Pulse shape discrimination cut for the neutron selection in the data from neutron detectors. Due to the stand type of the detector, there is few shielding for the neutron detector. So gamma backgrounds from the environment and cosmic rays make significant coincident triggers by chance.

Fig. 2.7 shows a 2-D plot for our PSD value and E_{meas} of every event from each neutron detectors. PSD value is defined as the ratio between the tail ADC sum and the total ADC sum, where the tail part is defined as "the total ADC sum – the ADC sum for the biggest pulse". Events above the PSD function are neutron events, and events below the function are gamma events.

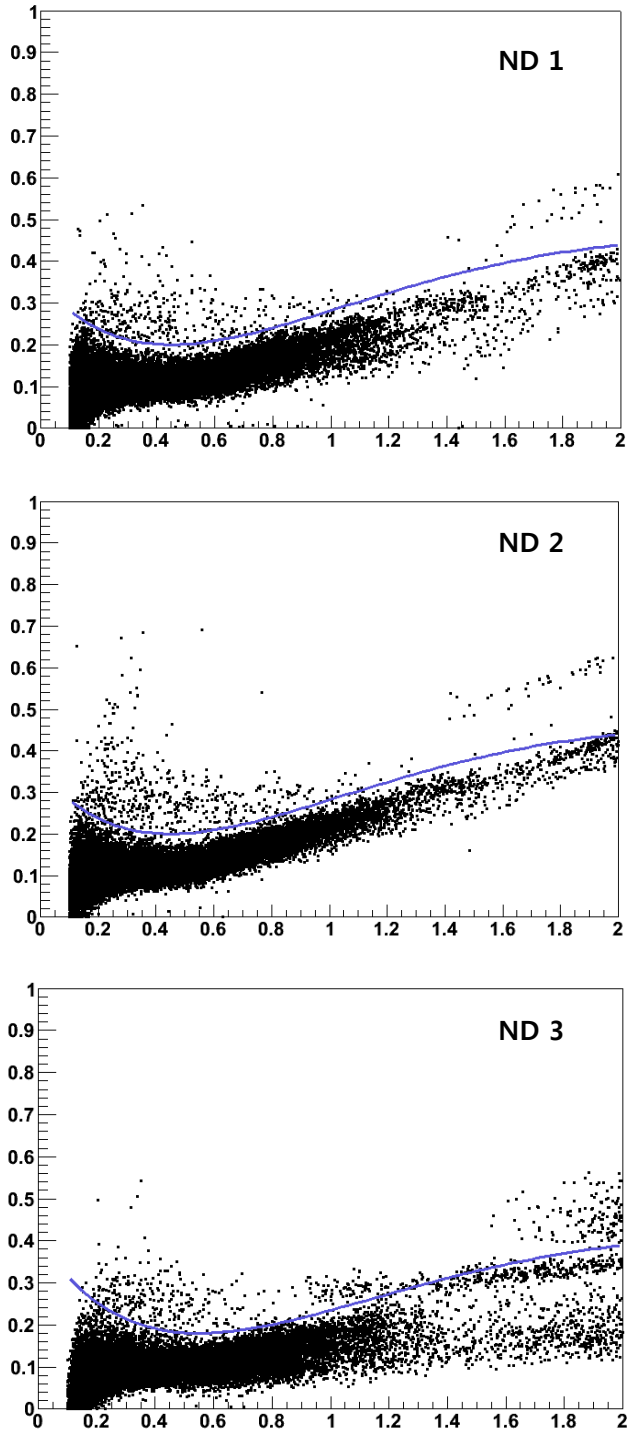

Figure 2.7 : Example of the pulse shape discrimination plot for three neutron detectors. The vertical axis represents the PSD value, and the horizontal axis represents the total ADC sum for each detector.

Chapter 3

Simulation

We did simulations to compare with the data obtained from our experimental setup, by two kinds of computer simulations, MARLOWE and Geant4.

3.1. MARLOWE

MARLOWE is the computer simulation program for atomic collisions in crystalline solids with the impulse approximation, which means that the binding forces on the target particle during the collision are ignored. Since it is open source code program written in FORTRAN, the user can generate output files containing all variables of interest and it can freely construct a crystal structure as we want [14]. We used MARLOWE to obtain the energy loss distribution of the ions in a material for each penetration depth. This information is a dominant factor to determine the scintillation yield of the crystal detector as mentioned in [15] [16] [17].

We constructed structure of the CsI(Tl) crystal by input file like Fig. 3.1, which is based on the previous simulation for the channeling effect in CsI(Tl) crystal done by Dr. Ju-hee Lee [12]. This crystal has mono-crystalline layer (POLY=0), and has primitive lattices (CENTRE=1) with lattice constant 4.5670 (ALAT=4.5670). There is two types of lattice sites, one is occupied by Cs whose fraction is 0.99927 (ORDER(1,1)=0.99927) and by Tl whose fraction is 0.00073 (ORDER(3,1)=0.00073), and the other is occupied by I

whose fraction is 1 (ORDER(2,2) = 1). In this simulation, thermal displacements of the lattice atoms is allowed by &TVIB option. Target temperature is 291.15K and the Debye temperature for each lattice sites is 115.08K. The initial kinetic energy of the primary recoil is 18,400 eV (EKP=18400) and initial direction of recoil is selected isotropically The initial location of the first primary recoil and the location of lattice site at (or near) which the first primary recoil starts is given by RAIP and REFIP in units of BASE (or its square), which is the computational unit length in the units of Ångströms. In order to make a simulation that is similar to an experimental setup, we assume that the incident theta has $\pm 5°$ divergence (DVRG=5.0). The beam is distributed isotropically within this interval

```
Channeling-Solid angle
with various energies
&MODL FILE(1)="file1.lst",FILE(2)="file2.lst",FILE(3)="file 3.lst",FILE(4)="l10Oslx1isa",FILE(5)="file5.lst"
      ,RDNML(1)=T,RDNML(3)=T,RDNML(5)=T,RDNML(6)=T,SURFCE=1,TRAM=F,ICHAN(1)=10000000,TIM=F,F,F,T,T,T,T/
&XTAL NEWS=4,ALAT=4.5670,CENTRE=1,RZ=3*0.0,3*0.5,POLY=0,AXISA=1.0,0.0,0.0,AXISB=0.0,1.0,0.0/
&ATOM NTYPE=3,TYPE='Cs','I','Tl',Z=55,53,81,W=132.905,126.904,204.383,INEL=3*2,EQUIT=3*6.3,EBND=6.3,0.6,0.6,
      6.3,0.6,0.6,6.3,0.6,0.6,LOCK(1)=-1,LOCK(2)=2,ORDER(1,1)=0.99927,ORDER(3,1)=0.00073,ORDER(2,2)=1/
&SURF ORIGIN=100.,100.,SIDES=1.0,1.0,RSRF=0.0,0.0,DEPTH=2E15,SBND=0.6,0.6,0.6/
&SIZE RB(1)=0.83,XILIM(1)=0.492373/,XILIM(3)=0.5,SLICE=0.0/
&QPAR ALPHA=3*0.7/
&TVIB T=298.0,TDEBYE=3*115.08/&TVIB T=298.0,TDEBYE(1)=38.,TDEBYE(2)=0.,TDEBYE(3)=78.5/
&OUTP DRNG=3*0.25,GREX=T,LOOK=1,TRACE=0,0,0,INFORM(1)=T/
&PROJ MAXRUN=100000,NGR=1,PRIM=0,EKIP=18400,LEAP=3,LAIP=2,RAIP=100.5,100.5,0.5,TRMP=F,MILLER=F,
      REFIP=100.5,100.5,0.5,THA=0.0,PHI=0.0,DVRG=20.0/
```

Figure 3.1 : An example of an input parameters used in MARLOWE simulation.

Our main purpose of simulation with MARLOWE is to compare its result with E_{meas}, which is the measured energy in the experiment, inferred from the scintillation light yield from the scintillation crystal, CsI(Tl). We reproduced E_{meas}in the mono-crystalline target from information of the deposit energy and a scintillation model from incident ion energy. To reproduce E_{meas}, first, we generate events with ions from a lattice point above. And second, divide the penetration depth along the initial direction into a unit depth and calculate the summed electronic stopping power. Then we can obtain E_{meas} as Eq.3.1 with an assumption that $\frac{L_\gamma}{E_\gamma}$ or $\frac{L_e}{E_e}$ is 1, where $L_{\gamma\ or\ e}$ is the light yields of gamma and $E_{\gamma\ or\ e}$ is the energy of gamma. [12]

$$E_{meas} = A \sum_{i=1}^{max.depthbin} \Delta E_{e,i}\ S(\frac{dE_{e,i}}{dx_i}) \qquad (3.1)$$

Where A is a normalization factor, $\Delta E_{e,i}$ is an electronic energy loss for i-th depth bin, and $S(\frac{dE_{e,i}}{dx_i})$ is scintillation efficiency for i-th summed electronic stopping power.

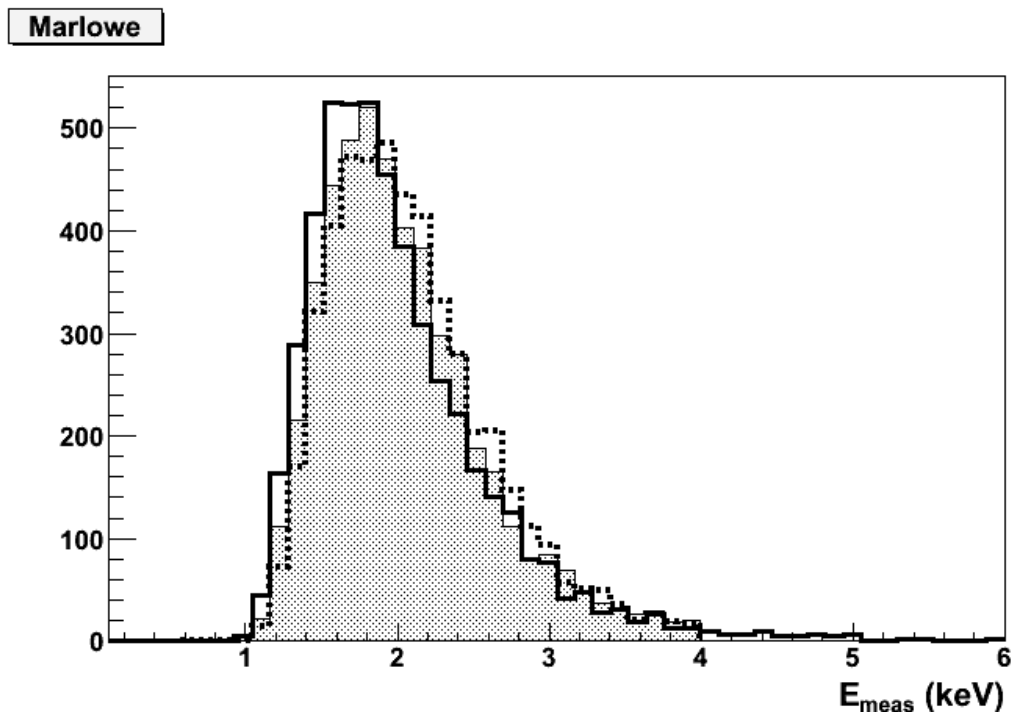

Figure 3.2 : Reproduced $\boldsymbol{E_{meas}}$ from MARLOWE simulation from 0 to 6 keV with different recoil directions. Thick solid line shows $\boldsymbol{E_{meas}}$ when angle between the (110) direction and recoil direction is 0°, and shaded one shows $\boldsymbol{E_{meas}}$ when the angle is 20°, and dotted line shows $\boldsymbol{E_{meas}}$ when the angle is 25°**.**

Fig.3.2 shows the reproduced $\boldsymbol{E_{meas}}$ from MARLOWE for each recoil direction. In the case of thick solid line, initial direction of the recoil is same with the (110) direction of the crystal, and events for shaded one and dotted line, angle between the (110) direction and initial direction of the recoil is 20° and 25°, respectively. Mean values and the sigma of the peak position for each case are listed in Table 4.1.

Fig.3.3 shows the reproduced $\boldsymbol{E_{meas}}$ with different temperature, 291K and 298K, for each recoil direction mentioned above.

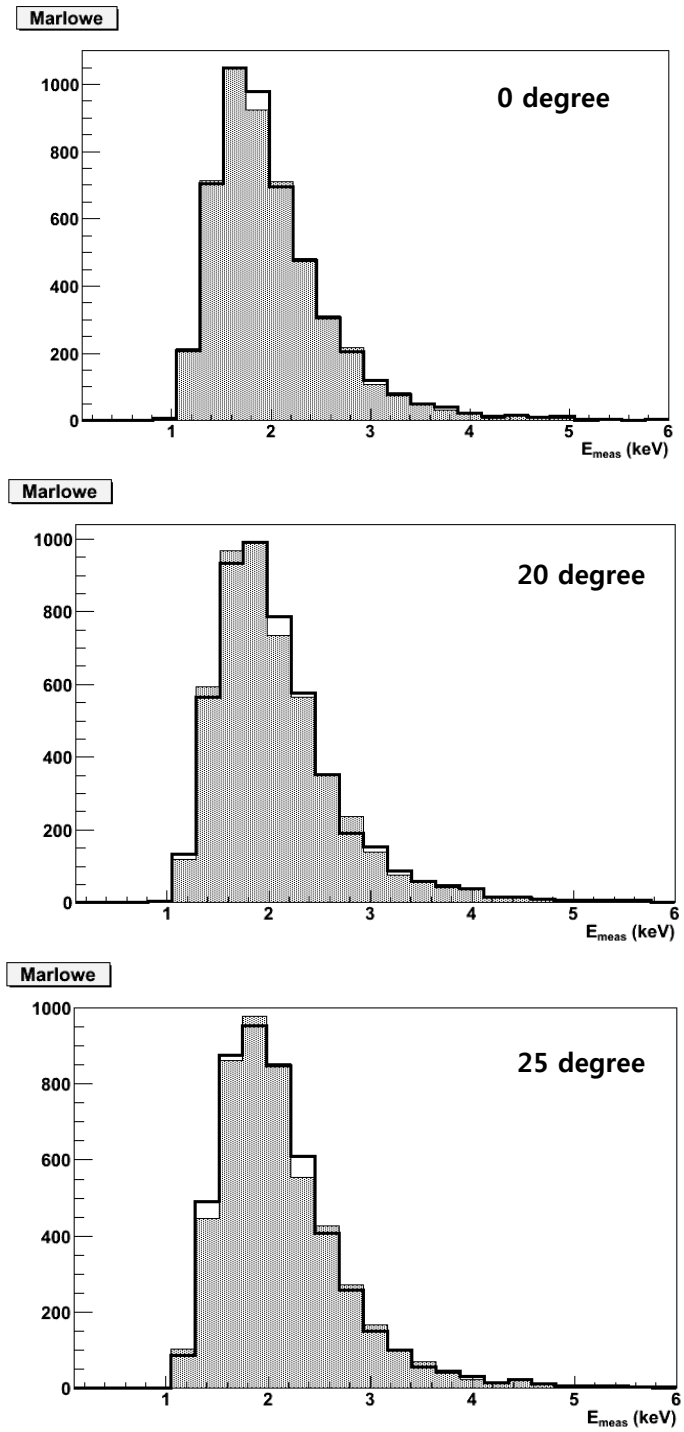

Figure 3.3 : Reproduced $\boldsymbol{E_{meas}}$ from MARLOWE simulation from 0 to 6 keV with different recoil directions. We compared two cases, setup with temperature of our experimental setup (291K, thick solid line), and with room temperature (298K, shaded one).

3.2. Geant4

Geant4 (for **GE**ometry **AN**d **T**racking) is a C++ based platform for "the simulation of the passage of particles through matter" using Monte Carlo methods, and is developed by CERN. Application areas include high energy physics and nuclear experiments, medical, accelerator and space physics studies. [18] Different with the MARLOWE, which is concentrated in constructing structure of the crystal and describing events inside the crystal, Geant4 can construct all of the environments we are interested in like Fig. 3.4.

When the events from the simulation satisfy the conditions below simultaneously, the events are selected as neutron scattering events.

- Deposit energy in CsI(Tl) > 0
- Gamma energy from the inelastic scattering in CsI(Tl) > 50 keV [a]
- X keV < $E_{meas,neutron}$ in the neutron detector [b] < Y keV
- No contribution in E_{meas} by gamma in the neutron detector
- Only one neutron detector has E_{meas} larger than 0

[a] When there is a transition from L shell to K shell in a nucleus, the gamma energy from Cs is 79.6 or 80.9 keV and from I is 57.6 keV. But in GEANT4 emits lower energy gammas for the energy conservation in the G4NeutronHPFinalState. We do not include those events.

[b] E_{meas} is calculated by the sum of Eq. 3.2. Since we use the ADC sum cut from 0.2 to 0.8 for the pulses detected by neutron detectors in the experiment, by comparing the ADC sum at 477.3 keV in the measurement, we determine X and Y.

$$E_{meas,neutron} = 0.83P - 2.82[1 - \exp(-0.25P^{0.93})] \quad \text{(Eq.3.2)}$$

where P is the proton energy obtained by an elastic scattering with a neutron.

Fig.3.5 shows the reproduced $\boldsymbol{E_{meas}}$ from Geant4 for each recoil direction. Thick solid line shows the reproduced $\boldsymbol{E_{meas}}$ when neutron particle is tagged by neutron detector 3 at Φ = 0°, and shaded one shows the reproduced $\boldsymbol{E_{meas}}$ when neutron particle is tagged by neutron detector 2 at Φ = 20°, and dotted one shows the reproduced $\boldsymbol{E_{meas}}$ when neutron particle is tagged by neutron detector 1 at Φ = 25°. Peak position and the sigma value of the peak for each case are listed in Table 4.1.

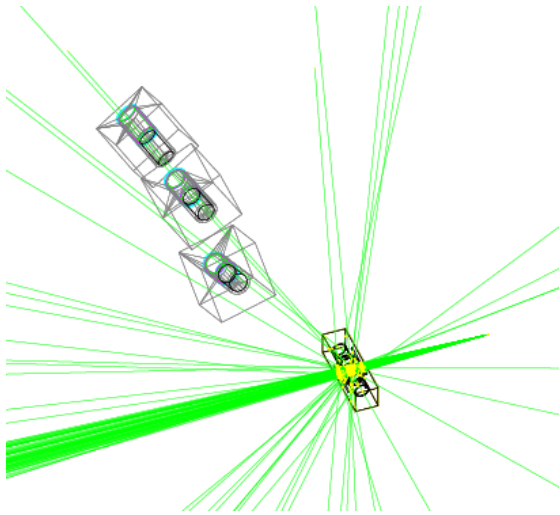

Figure 3.4 : Drawn simulation setup by GEANT4. Spreading lines shows path of the neutrons

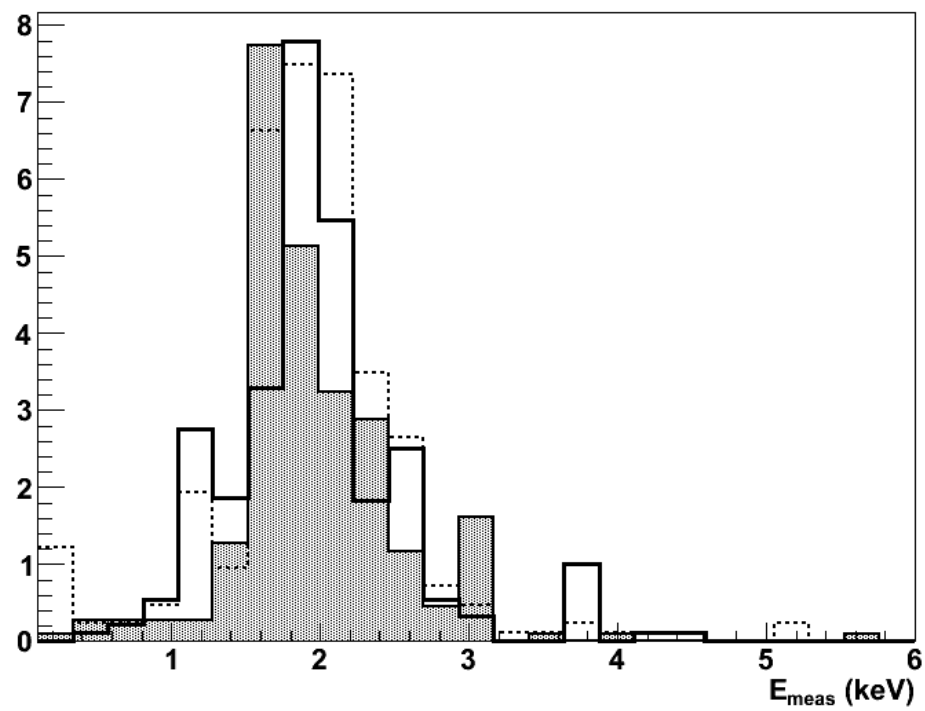

Figure 3.5 : Reproduced $\boldsymbol{E_{meas}}$ from Geant4 simulation from 0 to 6 keV with different recoil directions. Thick solid line shows $\boldsymbol{E_{meas}}$ when neutron is tagged by neutron detector 3 at Φ = 0°, and shaded one shows $\boldsymbol{E_{meas}}$ when neutron is tagged by neutron detector 2 at Φ = 20°, and dotted line shows $\boldsymbol{E_{meas}}$ when neutron is tagged by neutron detector 1 at Φ = 25°

Chapter 4

Data Analysis & Result

To measure the channeling and blocking effect, we measure E_{meas} in the case that directions of recoil ions are aligned along a symmetry axis, [110], and in other cases, the directions are aligned along random axes. The difference between them can be explained one of those effects. In this chapter, we compared the measured energies from our experiments and those from MARLOWE and Geant4. Moreover, we compared mean decay time of signals from our experiments.

After event selection in section 2.3, we can get some events which are candidates of nuclear recoils. Fig. 4.1 (a) is a histogram of measured energies of those events, from 0 keV to 100 keV. The measured energy is calculated from the scintillation yields recorded by two PMTs at both side of the CsI(Tl) crystal when there is a coincidence trigger between signals from PMTs and signals form one of the three neutron detectors. Most of the events are concentrated in the region that energy is lower than 20keV, especially near 2 keV. These events are pure elastic scattering events from collision between neutron and Cesium ion or neutron and Iodide ion. Fig. 4.1.(b) is a same histogram with Fig. 4.1 (a), with different energy range from 20keV to 100keV, there are three kind of events. We already know where events near 60 keV and 80 keV came from. [12] Events near 60keV are inelastic scattering events from collision between neutrons and Iodide ions and events near 80keV are inelastic scattering events from collision between neutrons and Cesium ions. But events near 30keV are not

completely confirmed yet. We suspected these events as X-ray from the neutron source, Zirconium, so we tried to remove these events by blocking neutron beam line by 2.5 cm lead block, as mentioned in Chapter 2. After blocking, almost of these near 30keV events are disappeared.

After applying PSD cut, these events are divided into three kinds of event, and their measured energies recorded by PMTs are tagged as Ech, Enon1, and Enon2 depend on their recoil direction. In Fig. 4.2, we compared each measured energy, Ech, Enon1, and Enon2 from the present experiment and those from the previous experiment. Fig. 4.2.(a) is a histogram of Ech, which is the energy of the CsI(Tl) crystal recorded by two PMTs when neutron comes into neutron detector 3, from 0.1keV to 6keV. Because when neutron comes into other neutron detectors, detector 1 or 2, Ech value becomes zero, it starts from 0.1 keV. There were total 238 events in from 0.1 to 100 keV, and total 205 events in from 0.1 to 6 keV. Fig. 4.2.(b) and Fig.4.2.(c) are histograms of Enon1 and Enon2, which is the energy of the CsI(Tl) crystal recorded by two PMTs when neutron comes into neutron detector 1 and 2 respectively, from 0.1keV to 6keV. For the same reason of the case of Ech`s, it starts from 0.1keV. For Enon1, there were total 214 events in from 0.1 to 100 keV, and total 205 events in from 0.1 to 6 keV. For Enon2, there were total 355 events in from 0 to 100 keV, and total 274 events in from 0.1 to 6 keV. Enon2 shows more events than others, because there is an coincidence between charge sum of neutron detector 1 and Enon2, which is the energy of the CsI(Tl) crystal when neutron comes into neutron detector 2.

In Fig.4.3 and Fig.4.4, we compared the each measured energy from the present experiment and those from the MARLOWE and Geant4. The reproduced measured energies from simulation with the recoil angles of 0°, 25°, and 20° correspond to the Ech, Enon1, and Enon2 of our experimental result, respectively. Table 4.1 shows peak position and sigma values of the first peak near 2 keV for each case.

Fig. 4.5 shows rmt10 value for Ech, Enon1 and Enon2 events with different energy range. rmt10 means charge weighted mean decay time for clusters within 10 μs. We can obtain information about how fast scintillation decays from rmt10. We expect lower rmt10 value when the blocking effect

occurs, because when the blocking effect occurs, signals of the events would decay in short time. In Fig. 4.6, we compared rmt10 values from the present experiment and those from the present experiment for Ech, Enon1 and Enon2 events. Their mean and sigma values are listed in Table 4.2.

Fig. 4.7 is a 2D-plot for rmt10 and energies of Ech, Enon1 and Enon2 events, and Fig. 4.8 is a 2D-plot for ndt0 and energies of Ech, Enon1 and Enon2 events. ndt0 means time difference between PMT`s signal and neutron detector`s signal in unit of μs. Generally, the time difference between two signals is about 0.2 μs.

		Present experiment	Previous experiment	MARLOWE Simulation	Geant4 Simulation
Ech	E_{peak}	1.454 ± 0.039	1.606 ± 0.059	1.745 ± 0.010	1.894 ± 0.010
	σ	0.371 ± 0.053	0.318 ± 0.042	0.380 ± 0.015	0.456 ± 0.010
Enon1	E_{peak}	1.634 ± 0.045	1.815 ± 0.065	1.872 ± 0.015	2.001 ± 0.081
	σ	0.542 ± 0.045	0.546 ± 0.051	0.472 ± 0.029	0.373 ± 0.009
Enon2	E_{peak}	1.649 ± 0.039	1.787 ± 0.052	1.853 ± 0.011	1.689 ± 0.082
	σ	0.559 ± 0.042	0.506 ± 0.045	0.449 ± 0.017	0.134 ± 0.004

Table 4.1 : Peak position and sigma value of first peak near 2 keV of Ech, Enon1 and Enon2, for each case

		Present experiment		Previous experiment	
Energy range		**0 to 6 keV**	**0 to 100 keV**	**0 to 6 keV**	**0 to 100 keV**
Ech	**Mean**	1.397 ± 0.045	1.429 ± 0.046	1.275 ± 0.046	1.308 ± 0.046
	σ	0.472 ± 0.037	0.531 ± 0.058	0.541 ± 0.039	0.559 ± 0.039
Enon1	**Mean**	1.349 ± 0.049	1.447 ± 0.056	1.310 ± 0.054	1.349 ± 0.064
	σ	0.531 ± 0.053	0.637 ± 0.065	0.564 ± 0.051	0.644 ± 0.070
Enon2	**Mean**	1.337 ± 0.040	1.399 ± 0.034	1.310 ± 0.060	1.345 ± 0.080
	σ	0.539 ± 0.040	0.552 ± 0.033	0.587 ± 0.054	0.735 ± 0.100

Table 4.2 : Mean and sigma value of rmt10 for Ech, Enon1 and Enon2 event.

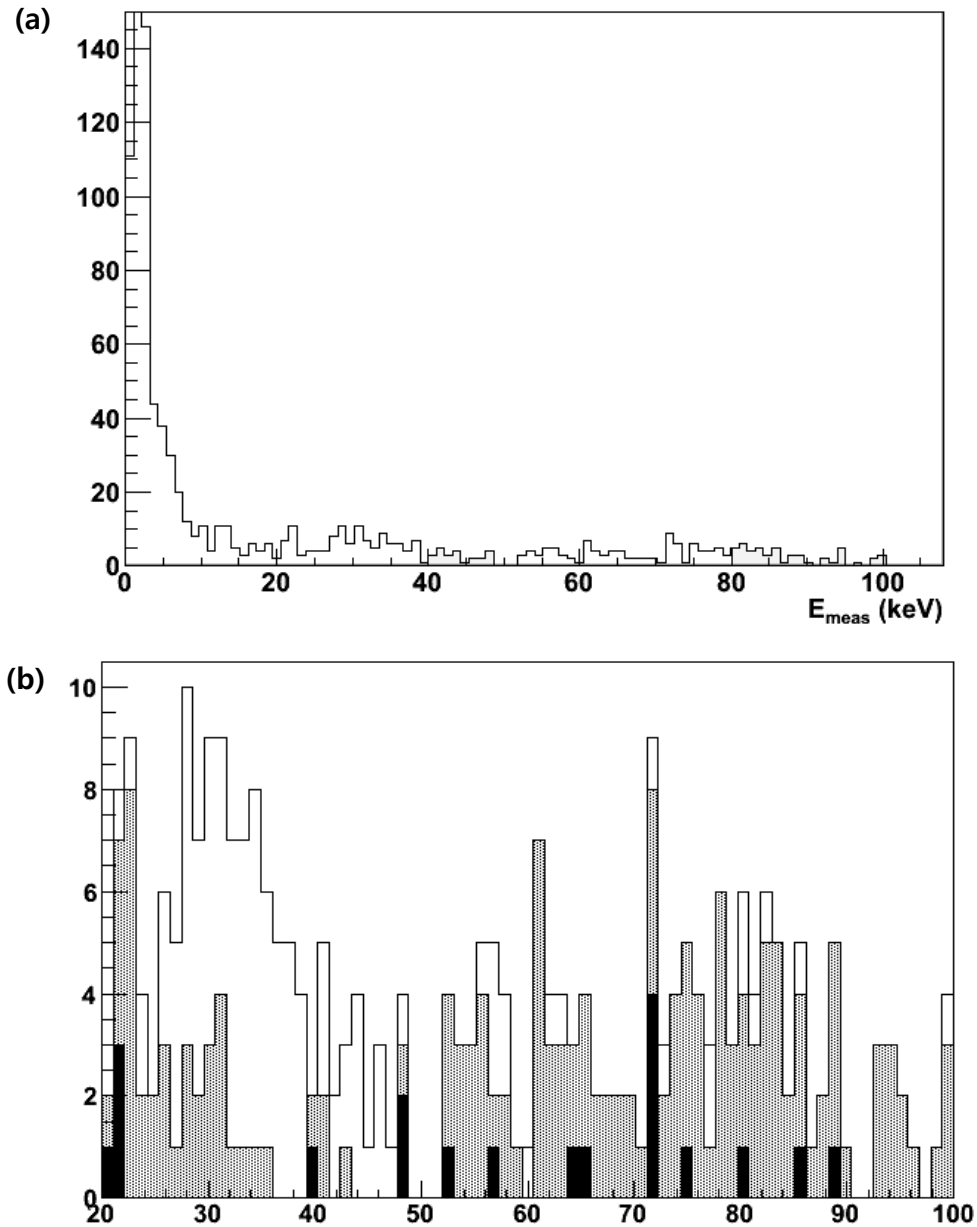

Fig. 4.1 : histogram of measured energies from 0 to 100 keV (a), and from 20 to 100 keV (b), recorded by three neutron detectors and PMTs. In Fig. 4.1.(b), solid line is events from overall data, and shaded one is events from after blocking beam line with lead block as Fig.2.1.①. Filled with black one is events from after putting some more lead blocks as Fig.2.1.②.

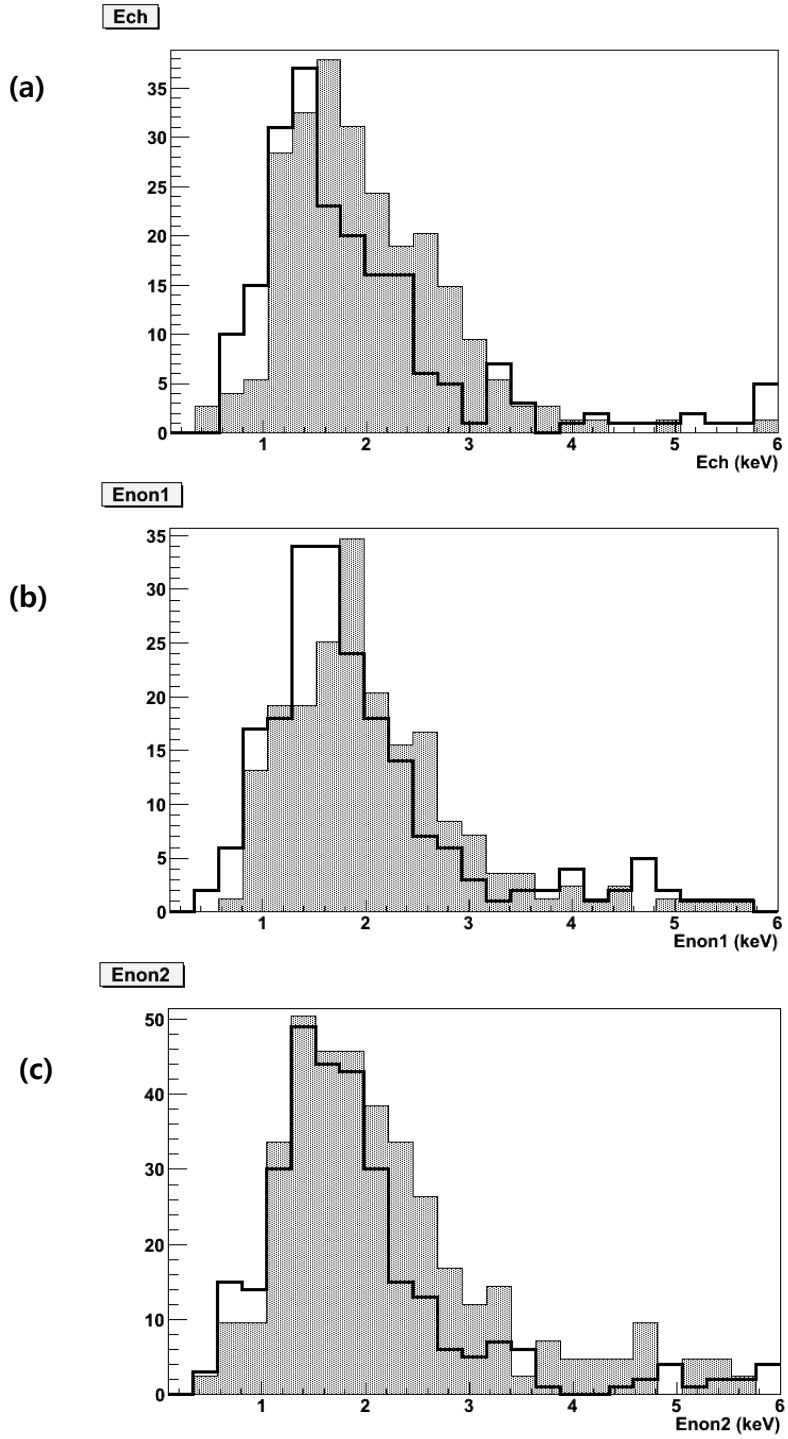

Figure. 4.2 : Histograms of Ech (a), Enon1 (b), and Enon2 (c). Solid line shows events from present experiment, and shaded one shows events from Dr. Ju-hee Lee`s data

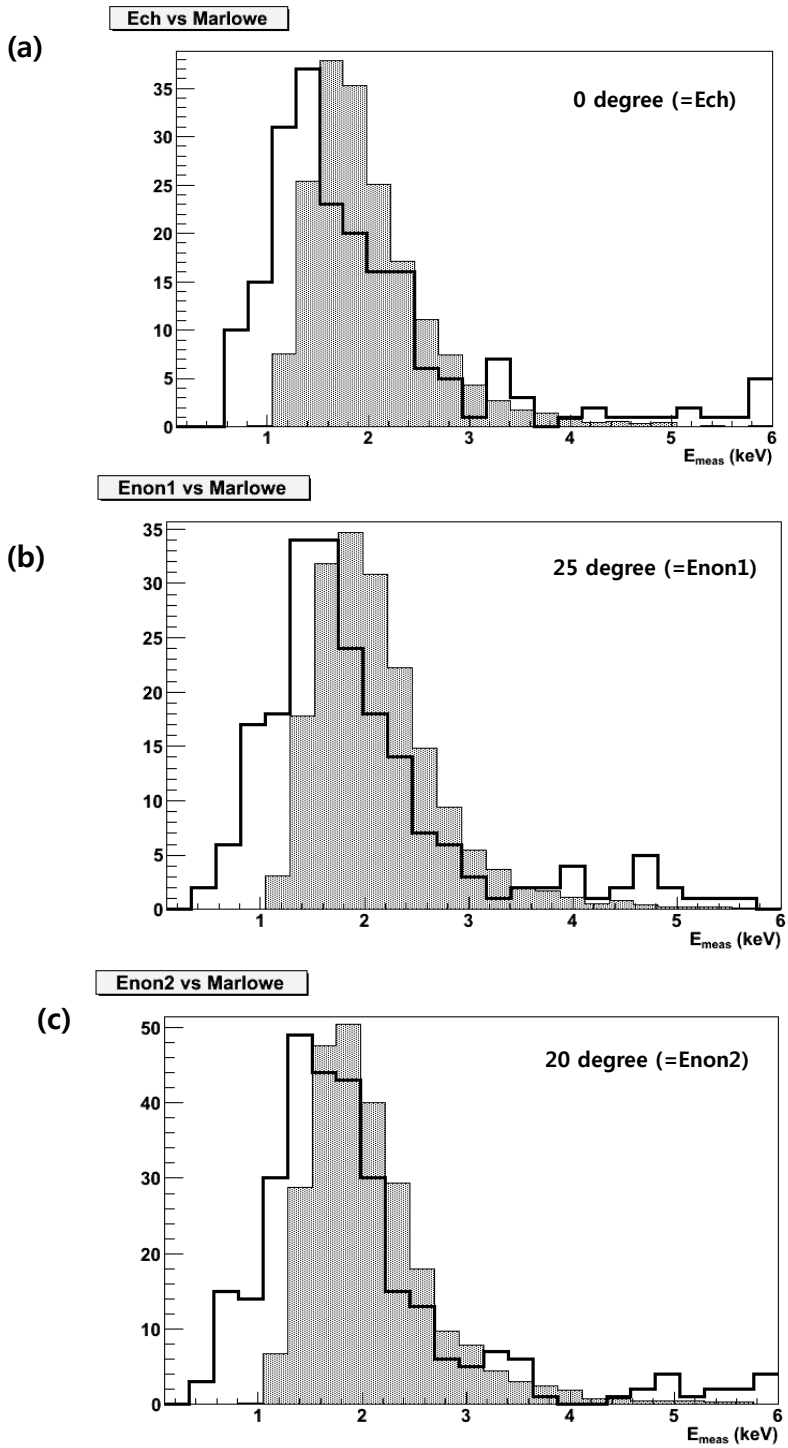

Figure 4.3 : Comparison between experimental measured energy data and reproduced E_{meas} from MARLOWE simulation from 0 to 6 keV. Solid line is events from experimental data, and shaded one is events from Geant4 simulation.

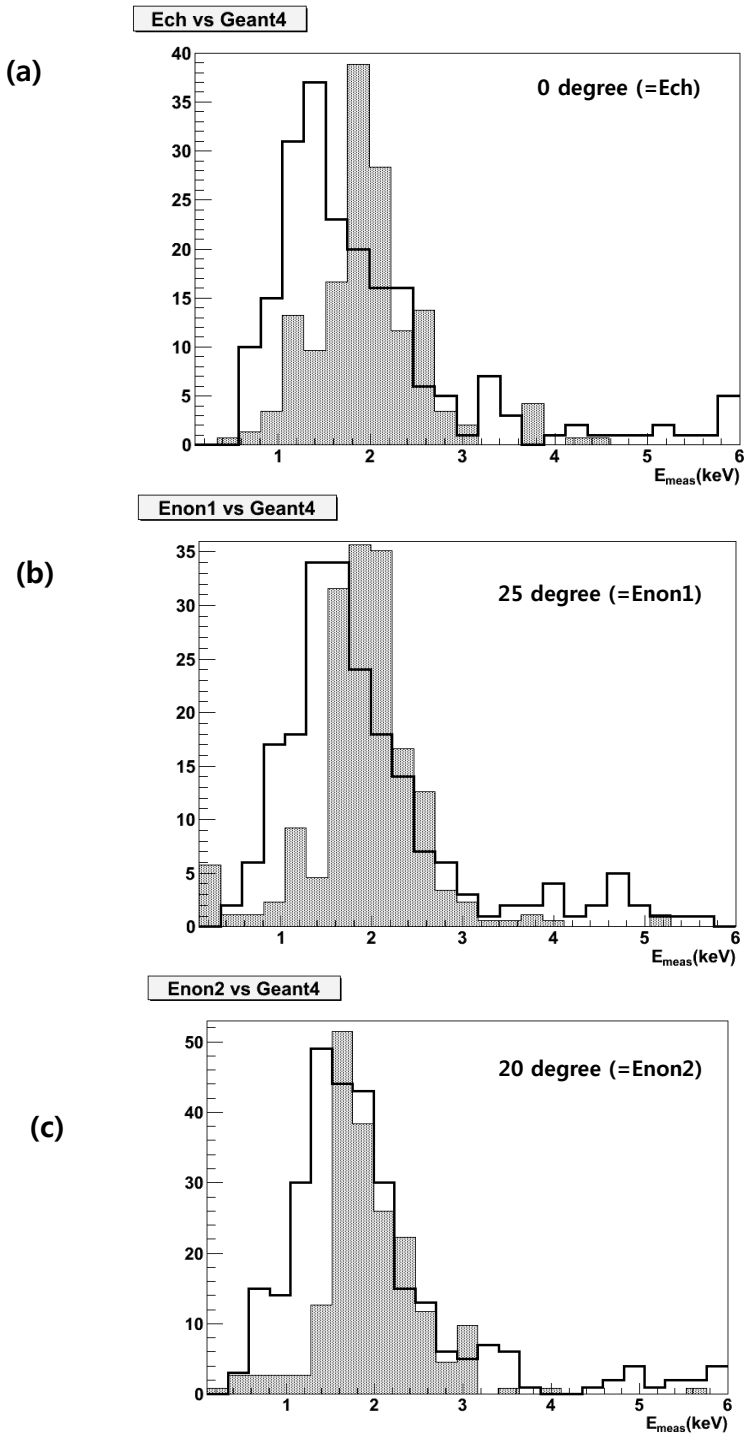

Figure 4.4 : Comparison between experimental measured energy data and reproduced E_{meas} from Geant4 simulation from 0 to 6 keV. Solid line is events from experimental data, and shaded one is events from Geant4 simulation.

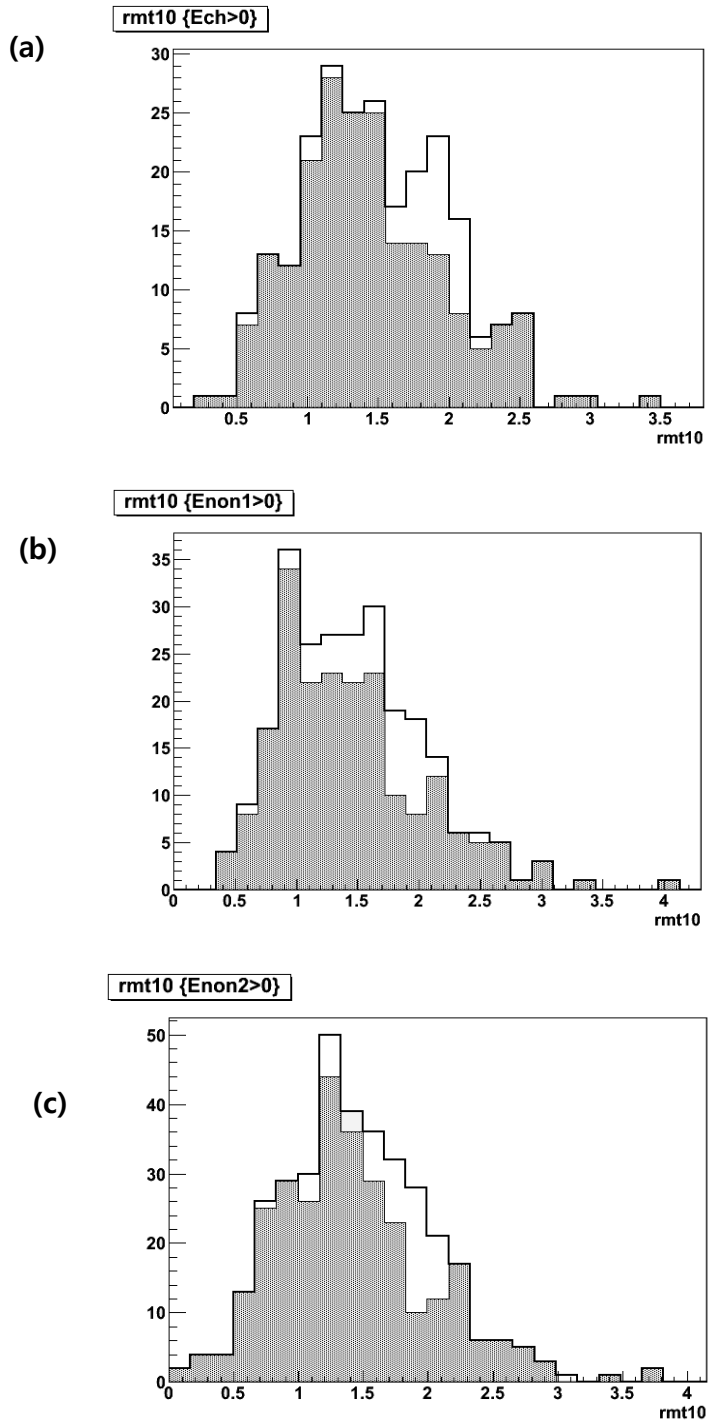

Figure 4.5 : Histogram of rmt10 for each measured energy, Ech (a), Enon1 (b), and Enon2 (c). Thick solid line shows event from 0 keV to 100 keV, and shaded one shows events from 0 keV to 6 keV.

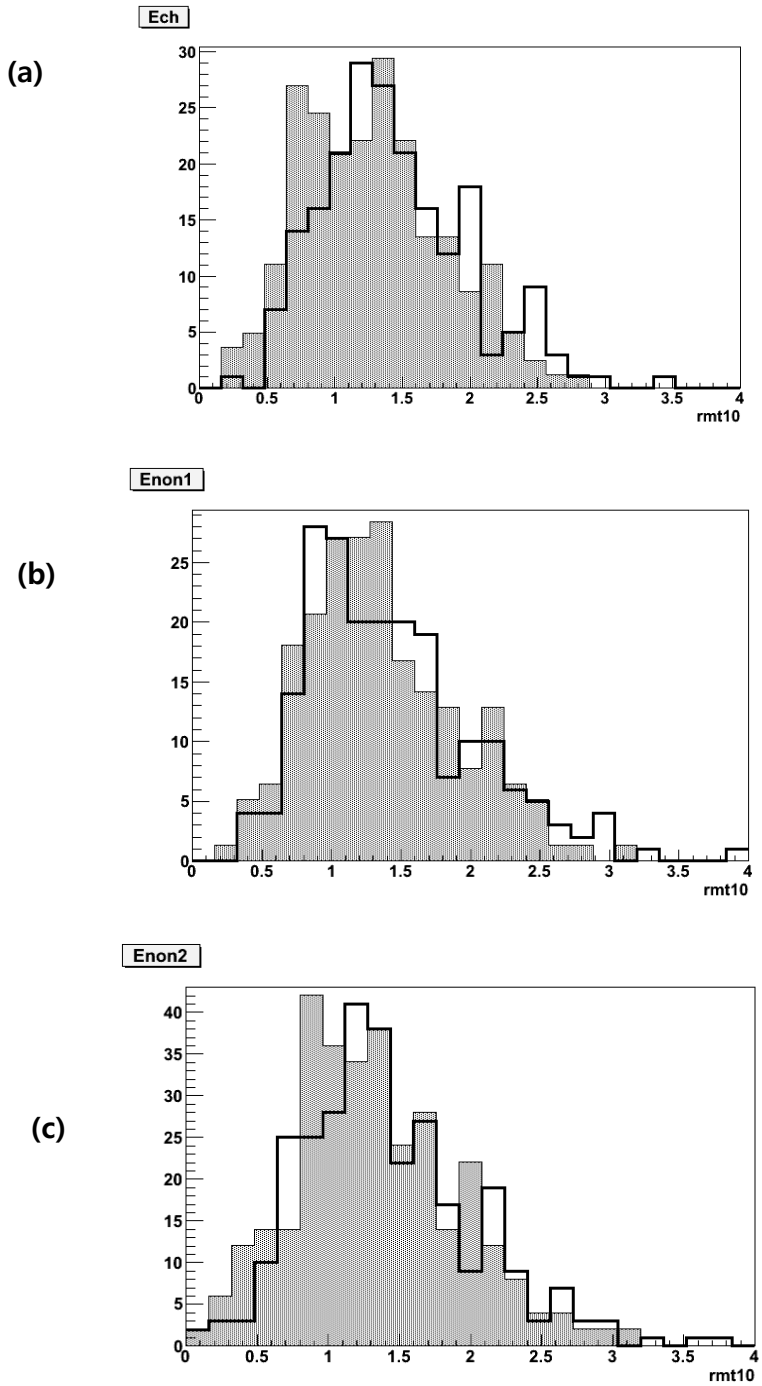

Figure 4.6 : Histogram of rmt10 for each measured energy, Ech (a), Enon1 (b), and Enon2 (c), from 0 to 6keV. Thick solid line shows event from present result, and shaded one shows events from previous result.

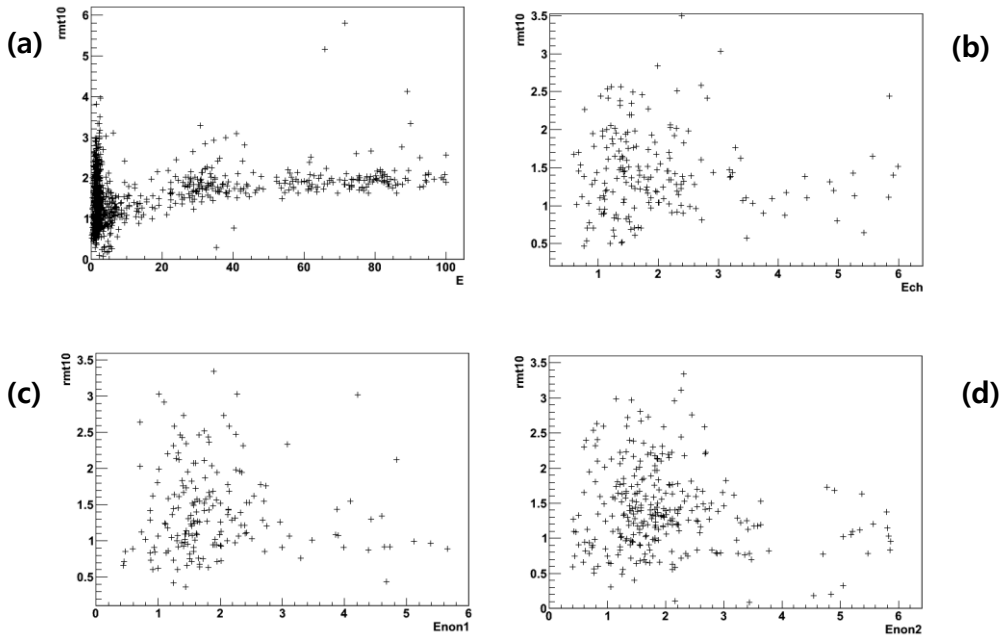

Fig. 4.7 : 2D plot for rmt10 and E for 0 to 100 keV (a), and Ech for 0.1 to 6 keV (b), and Enon1 for 0.1 to 6 keV (c), and Enon2 for 0.1 to 6 keV(d).

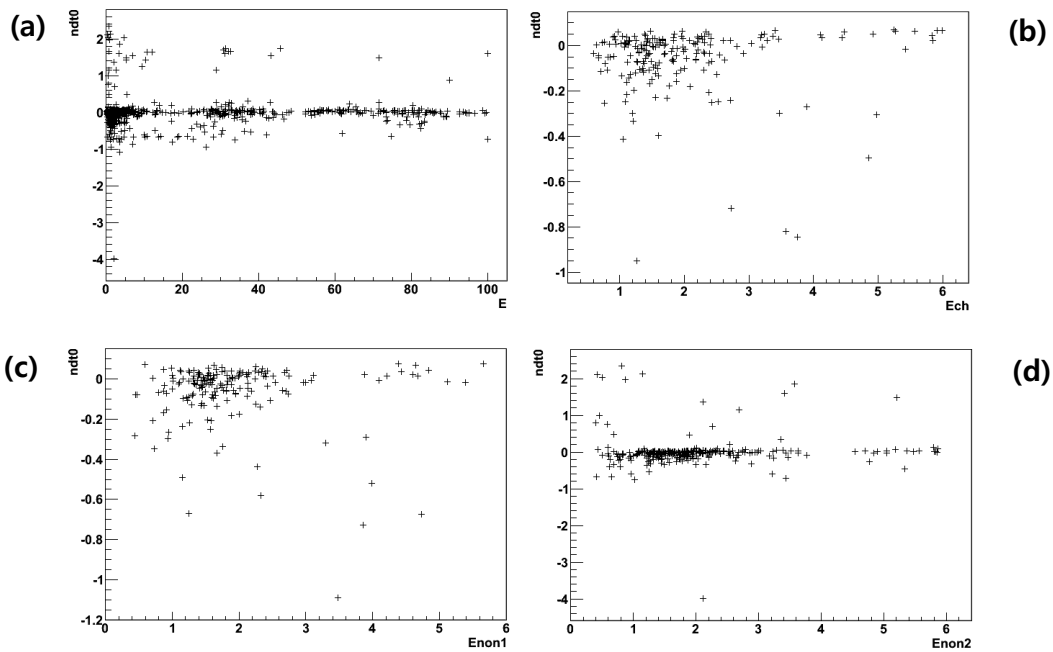

Fig. 4.8 : 2D plot for ndt0 and E for 0 to 100 keV (a), and Ech for 0.1 to 6 keV (b), and Enon1 for 0.1 to 6 keV (c), and Enon2 for 0.1 to 6 keV (d).

Chapter 5

Conclusion

As mentioned in section 1.3, our study starts from the claim by DAMA that KIMS detector loses some nuclear recoil events because of the channeling effect and their pulse shape discrimination (PSD) cut. But in their study, they overestimated the channeling fraction because they did not consider the blocking effect. The main purpose of this study is to investigate the fraction of blocking effect and affection of the blocking effect on scintillation yield from the CsI(Tl) crystal. To study about those, we decided to study about the channeling and blocking effect on the CsI(Tl) crystal. We constructed experimental setup to measure the channeling and blocking effect and we did simulations with two kinds of computer simulation programs, MARLOWE and Geant4, to reproduced the channeling effect on the CsI(Tl) crystal by recoil ions.

To confirm the affection of the blocking effect on scintillation yield from the CsI(Tl) crystal, we compared each measured energy, Ech, Enon1, and Enon2 from the present experiment with those from the Dr. Ju-hee Lee`s previous experiment in Fig. 4.2, and with reproduced measured energies from two kinds of simulations, MARLOWE and Geant4, in Fig. 4.3 and in Fig. 4.4. Also, we compared peak and sigma value of first peak, near 2 keV, for each case. The result is listed in Table 4.1. As shown in the table, Ech value from the both experiments is about 10% lower than Enon1 and Enon2 value. We expect this difference is result from the blocking effect, which reduces scintillation yield by large-angle scattering.

Also, we compared rmt10 values from the result of present experiment with the results from previous experiment for Ech, Enon1, and Enon2 event in Fig.4.5. Their mean and sigma value is listed in Table 4.2. We expect lower rmt10 value when the blocking effect occurs, because when the blocking effect occurs, signals of the events would decay in short time, but we cannot see significant differences in the Table 4.2.

As we mentioned above, we could find a clue for the affection of the blocking effect on scintillation yield from the CsI(Tl) crystal by comparing Ech, Enon1 and Enon2. However, we need more study about the differences in measured energy between the results of the present experiment and the results of the previous experiment. Moreover, we need more study about no significant differences in rmt10 values of Ech, Enon1 and Enon2 events from the result of the present experiment, as shown in Table 4.2. After understanding those, we will be able to find a clue to understand the blocking effect in the CsI(Tl) crystal.

Bibliography

[1] Ade, P. A. R.; Aghanim, N.; Armitage-Caplan, C.; et al., “Planck 2013 results. I. Overview of products and scientific results” arXiv:1303.5062. Bibcode:2013arXiv1303.5062P

[2] F. Zwicky. Republication of: “The redshift of extragalactic nebulae. General Relativity and Gravitation” 41, 207, 2008 English version of Helv. Phys. Acta 6, 110 (1933).

[3] H. S. Lee. “Dark Matter Search with CsI(Tl) Crystals” PhD thesis, Seoul Natioanl University, 2007.

[4] S. C. Kim. “Dark Matter Search with 100 kg of CsI(Tl) Crystals” PhD thesis, Seoul Natioanl University, 2011.

[5] H. Erramli and G. Blodiaux, “Ion channeling” Appl. Radiat. Isot. 46 (1995) 413.

[6] J.U.Andersen et al., “Attosecond time delays in heavy-ion induced fission measured by crystal blocking” Phys. Rev. C 78 (2008) 064609

[7] C. Cohen and D. Dauvergne, “High energy ion channeling principles and typical applications” Nucl. Instrum. Meth. Phys. Res. B 225 (2004) 40.

[8] The University of Sheffield
“http://www.hep.shef.ac.uk/research/dm/intro.php”

[9] The Purdue University
“htp://www.physics.purdue.edu/darkmatters/blog/?m=20120822”

[10] DAMA collaboration R. Bernabei et al. “Possible implications of the channeling effect in NaI(Tl) crystals” Eur. Phys. J. C53, 2, 205, 2008.

[11] N. Bozorgnia et al. “Channeling in direct dark matter detection iii : Channeling fraction in CsI crystals”. JCAP 11, 029, 2010.

[12] J. H. Lee, “Channeling effect in the CsI(Tl) used for a WIMP search” PhD thesis, Seoul National University, 2012.

[13] Hamamatsu. “http://www.hamamatsu.com”.

[14] Abstract for MARLOWE by RSICC
“https://rsicc.ornl.gov/codes/psr/psr1/psr-137.html”

[15] R. B. Murray and A. Meyer. “Scintillation response of activated inorgarnic crystals to various charged particles” Phys. Rev., 122, 3, 815, 1961.

[16] A. Hitachi. “Properties of liquid xenon scintillation for dark matter searches” Astropart. Phys.24, 247, 2005.

[17] V. I. Tretyak. “Semi-empirical calculation of quenching factors for ions in scintillators” Astropart. Phys.33, 40, 2010.

[18] Geant4 “http://geant4.web.cern.ch/geant4/”

초 록

암흑 물질로 추정되는 물질들 중 가장 유력한 후보인 WIMP를 직접적으로 검출하기 위해 KIMS 연구 그룹은 CsI(Tl) 결정을 신틸레이션 검출기로서 사용했다. 이 검출기의 민감도를 향상시키기 위해, 우리는 CsI(Tl) 결정 내에서의 채널링 효과와 블로킹 효과에 대해 연구하기로 결정했다. 이 두 효과는 하전 이온의 결정 내에서의 이동 방향에 따라 관통 정도가 달라지는 것과 관련된 효과로, 이 효과들로 인해 CsI(Tl) 결정 내에서 신틸레이션과 이온화가 일어나는 양에 변화가 생기게 된다.

CsI(Tl) 결정 내에서의 채널링 효과와 블로킹 효과를 측정하기 위해, 우리는 중성자 발생장치, 중성자 검출기, 그리고 CsI(Tl) 결정을 이용해 중성자와 핵의 산란을 통해 튕겨져 나가는 이온이 CsI(Tl) 결정의 대칭축 혹은 대칭 평면의 방향으로 나아가도록 배치하였다. 또한, 실험으로부터 얻은 결과와 비교하기 위해 MARLOWE, Geant4 두 종류의 컴퓨터 시뮬레이션 프로그램을 사용하였다. 블로킹 효과가 CsI(Tl) 결정에 끼치는 영향을 알아보기 위해, 튕겨져 나간 이온이 [110] 대칭축을 따라 움직이는 경우와 임의의 방향으로 움직이는 경우에 신틸레이션으로 방출되는 빛의 양을 비교하였으며, 각각의 경우에 대해 신호가 사라지게 되는 평균 시간을 비교하였다. 실험과 시뮬레이션으로 얻어진 결과를 비교함으로써 우리는 신틸레이션으로 인해 방출되는 빛이 적어지게 될 것으로 기대되는 블로킹 효과에 대한 단서를 찾을 수 있었다.

주요어: 암흑 물질, WIMPs, KIMS, CsI(Tl) 결정, 채널링 효과,
블로킹 효과, 신틸레이션

학번 : 2011-23281